BOUNDARY LAYER RESPONSE TO ARBITRARY ACCELERATION

Combrinck M.L.*, Dala L.N. and Lipatov I.I.
*Author for correspondence
Department of Mechanical and Aeronautical Engineering,
University of Pretoria,
Pretoria, 0002,
South Africa,
E-mail: madeleine.combrinck@gmail.com

ABSTRACT

In this paper the response of the laminar boundary layer on a flat plate to arbitrary translation were investigated numerically. It was found that accelerating velocity profiles have steeper gradients in the near wall region and a lightly thicker boundary layer when compared to steady state results ([3],[15]). The gradient were proportional to the acceleration parameter. Decelerating velocity profiles indicated that flow reversal took place. This reversal was proportional to the deceleration. The boundary layer was thinner than calculated in the steady state case. Three types of responses of the boundary layer to changing conditions in the relative frame velocity have been identified; Response Type I which is viscous dominant, Response Type II where certain regions in the boundary layer are dominated by viscosity and other regions by momentum and Response Type III which is dominated by momentum.

INTRODUCTION

In this paper the response of the laminar boundary layer on a flat plate in arbitrary translation is investigated. This is done using a non-inertial approach as mathematically described for rotation cases in [5]. Formulations of the non-inertial conservation of momentum equation is available from literature [2], [10], [19]. Non-inertial studies mostly focussed on turbo-machinery, wind turbines and other studies that involves rotation [4], [13], [12]. A method was proposed by Kageyama and Hyodo [12] to derive the Coriolis force in the momentum equation using and Eulerian approach. While it only concerned incompressible flow in constant rotation, the approach was mathematically rigorous and was adapted in Combrinck et.al.[6] to account for the full aeroballistic range of motion - acceleration in six degrees of freedom. The set of Navier-Stokes equations that was formulated with this approach, were implemented in an numerical code and is used in this analysis. Two studies that bear specific relevance to this work is Mager [14] and [1]. These are used as benchmarks for the observed boundary layer behaviour.

NOMENCLATURE

e	Internal energy
h	Enthalpy
k	Heat transfer coefficient
p	Pressure
r_u	Gas Constant
t	Time
u	Velocity in the x-direction
u	Velocity vector
x	Displacement in the x-direction
x	Position vector
C_p	Specific heat at constant pressure
I	Identity matrix
M_w	Molecular Weight
P_r	Prandtl Number
R	Universal gas constant
T	Temperature
V	Velocity vector
X	Position vector

Special Characters

κ	Thermal conductivity
λ	Second viscosity
μ	Dynamic viscosity
ν	Kinematic viscosity
ρ	Density
ϕ	Viscous dissipation term
ψ	Specific pressure $\frac{p}{\rho}$
Ω	Rotational speed around the z-axis
$\mathbf{\Omega}$	Rotational speed vector
∇	Del operator

Subscripts and Superscripts

s	Static conditions
t	Total conditions

THEORETICAL FORMULATION

Assumptions

The following assumptions were made with regards to the flow field in this analysis:

- The flow can be completely described in the non-inertial reference frame.
- The fluid is Newtonian i.e. the viscous stresses in the fluid is linearly proportional to the strain rate.
- The ideal gas law is an appropriate equation of state to utilize at a closure model.
- The compressible form of the governing equations accurately describes the flow.
- The flow is well within the laminar regime, no turbulence

models are employed.
- Viscous dissipation terms, $\hat{\phi}$, in the energy equation can be neglected since this is a laminar case and the dissipation term is associated with turbulent behaviour.
- The bulk viscosity is zero, as per Stokes Law.
- Heat conduction is described by Fouriers Law.

Governing Equations

The governing equations used in the analysis was derived in [6]. The conservation of mass equation made use of the formulation:

$$\frac{\partial \hat{\rho}}{\partial t} + \hat{\nabla} \cdot \hat{\rho}\hat{\mathbf{u}} = 0 \tag{1}$$

The non-inertial energy equation was shown in [5] to have no non-inertial term, this was confirmed in [6].

$$\frac{\partial \hat{\rho}\hat{e}}{\partial t} + (\hat{\nabla} \cdot \hat{\rho}\hat{e}\hat{\mathbf{u}}) = -\hat{p}(\hat{\nabla} \cdot \hat{\mathbf{u}}) + \hat{\nabla} \cdot (\hat{k}\hat{\nabla}\hat{T}) + \hat{\phi} \tag{2}$$

The non-inertial momentum equation for fully arbitrary flow was implemented as follow:

$$\begin{aligned} &\frac{\partial \hat{\rho}\hat{\mathbf{u}}}{\partial t} + \hat{\nabla} \cdot (\hat{\rho}\hat{\mathbf{u}} \otimes \hat{\mathbf{u}}) - \hat{\nabla} \cdot [\hat{\mu}(\hat{\nabla}\hat{\mathbf{u}} + \hat{\nabla}\hat{\mathbf{u}}^T) + \hat{\lambda}(\hat{\nabla} \cdot \hat{\mathbf{u}})\hat{\mathbf{I}}] \\ &\quad + \underbrace{\frac{\partial}{\partial t}(\rho \mathbf{V}(t))}_{\text{Translation}} - \underbrace{\rho\hat{\mathbf{x}} \wedge \dot{\mathbf{\Omega}}}_{\text{Euler}} - \underbrace{2\rho\hat{\mathbf{u}} \wedge \mathbf{\Omega}}_{\text{Coriolis}} \\ &\quad + \underbrace{\rho\hat{\mathbf{x}} \wedge \mathbf{\Omega} \wedge \mathbf{\Omega}}_{\text{Centrifugal}} - \underbrace{2\rho\mathbf{V}(t) \wedge \mathbf{\Omega}}_{\text{Magnus}} = -\hat{\nabla}\hat{p} \end{aligned} \tag{3}$$

Closure Models

The system of governing equations above requires additional equation to obtain a unique solution. An equation of state, transport model and thermodynamic model is required to ensure that for the number of unknowns, there are the same number of equations.

The equation of state used in this case is the ideal gas law. This relates the pressure to the density, gas constant and temperature of the fluid.

$$p = \rho RT \tag{4}$$

The transport model makes use the equation below, where the Prandtl number is expressed as a ratio of viscous diffusion rate over the thermal diffusion rate:

$$P_r = \frac{C_p \mu}{\kappa} \tag{5}$$

In this implementation either the internal energy or enthalpy can be used to determine the temperature profile in the fluid. The enthalpy is a function of internal energy and pressure. This equation can be re-written to make the internal energy the subject of the equation. The known quantities in the flow is then used to model the internal energy.

$$\begin{aligned} e_s &= h_s - \frac{p}{\rho} \\ &= \int_{T_0}^{T} C_p T - \frac{r_u T_0}{M_w} \end{aligned} \tag{6}$$

The total enthalpy can also be expressed as the sum of the static enthalpy and the enthalpy of the dynamic pressure ([17]). The static enthalpy is replaced with known quantities in the flow, and the equation becomes:

$$h_t = \int_{T_0}^{T} C_p dT + 0.5\mathbf{U} \cdot \mathbf{U} \tag{7}$$

CASE DESCRIPTION

Analysis Overview

The accelerating cases were initialized from a steady state solution at 10 m/s (Re = 3.5×10^4) and accelerated to a free stream velocity of 80 m/s (Re = 2.81×10^5). This was be done at for five cases each at acceleration speeds from 70g to 700000g with increasing orders of 10. The decelerating cases were initialized from a steady state solution of 80 m/s (Re = 2.81×10^5) and decelerated to 10 m/s (Re = 3.5×10^4) for five cases with varying constant decelerations from 70g to 700000g with increasing orders of 10.
The flow conditions were select to ensure that the fluid remains well within the laminar regime. To this effect the Reynolds number for a flat plate in translation must be below 300 000 ([7]).

The steady state boundary layer, in both the inertial and non-inertial frames, is depicted in Figure .

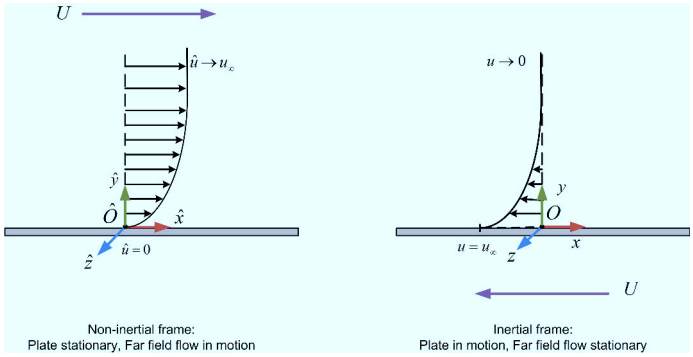

Figure 1. Graphical Representation of the Boundary Layer on a Flat Plate

In the inertial frame the plate is in motion with a velocity U in the negative x-direction. In the near-wall region the

boundary layer assumes an absolute velocity of U in the negative x-direction - the velocity at which the plate is moving. In the far field the absolute velocity approaches zero. In the non-inertial frame the perspective of the observer has changed; the plate is stationary and the fluid is in motion. In the near-wall region the fluid velocity approaches zero on the no-slip wall and in the far field the fluid velocity approaches U - the relative velocity of the moving plate. The difference between the two frames is best described as: in the non-inertial frame the plate is stationary and the fluid is in motion, while in the inertial frame the plate is in motion and the fluid is stationary.

Computational Domains

Computational grids are required with a sufficient amount of cells in the near-wall viscous region. It is good practise to design a grid to have at least 15 cells in the boundary layer region and for the first dimensionless cell node height to be in order of $y^+ = 1$ ([9]). The approximate boundary layer height was calculated. The estimated boundary region was populated with 50 cells with a first celll height of 2.6E-4 mm. The computational domain is described in Figure . The grid have been designed and tested to ensure grid independence (Figure 3).

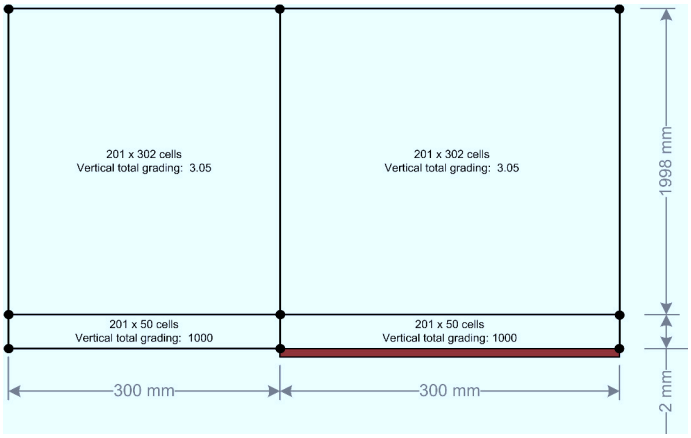

Figure 2. Computational Domain for Translating Plate Case

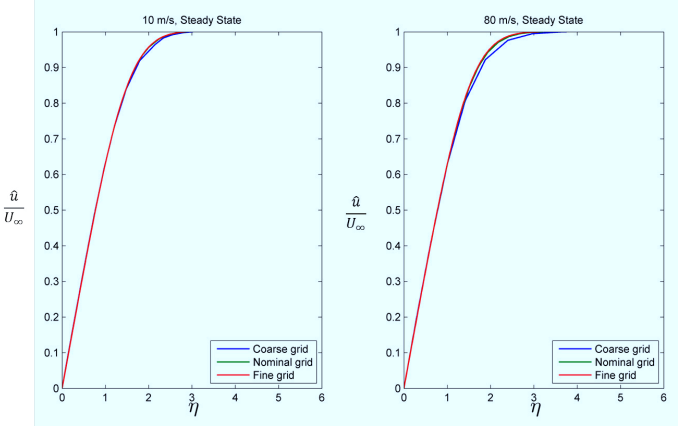

Figure 3. Grid Independence Study Results

Boundary Specification

The boundary condition locations for the flat plate is graphically represented in Figure 4. A specialized boundary condition was implemented on the far field velocity to ensure conservation on the non-inertial velocity field. The boundary conditions specifies the far field inertial velocity, which is stationary, and the code calculates the relevant non-inertial velocity using the prescribed motion of the moving frame. The flow conditions was select to ensure that the fluid remains laminar. To this effect the Reynolds number for a flat plate in translation must be below 300 000 ([7]).

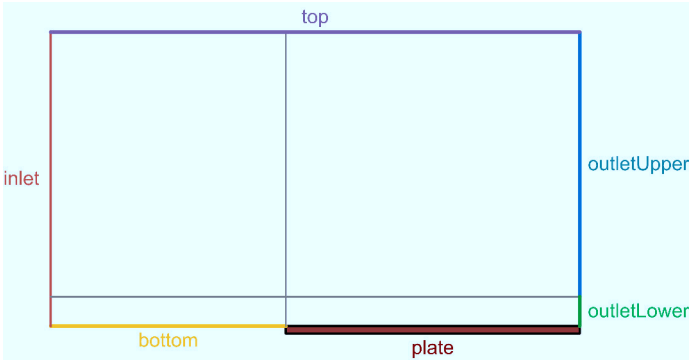

Figure 4. Graphical Representation of Translating Plate Boundary Condition

Numerical Method

The analysis were done in OpenFOAM ®([16]). It is a C++ toolbox that provides a platform for the development of customized numerical solvers related to continuum mechanics problems using the finite volume method. It is released under the Open Source Software GNU General Public License ([11]).

Time integration was done using the implicit Euler method ([9],[18]). In the steady state solutions the Courant number was kept below 0.9. In the accelerating and decelerating cases a constant time step were used since time accurate results are required.

Discretization of the divergence terms were done using Gausss theorem ([9],[18]) with a total variate diminishing scheme. The gradient and laplacian term terms were both discretised with Gausss theorem and a central differencing scheme ([9],[18]).

VALIDATION

The laminar, two dimensional, flat plate was used as a validation case. This case tested the functionality of the developed solver. The boundary layer on a flat plate is self-similar which means that along the plate the shape of the velocity distribution differs in scale but the form of the profile remains the same. The profile shape is also similar between the non-inertial and inertial frames, with the exception of directionality (Figure).

The laminar flat plate is a classic problem in Fluid Mechanics for which a similarity solution was developed by [3]. In a similar manner [15] derived a solution for laminar compressible bound-

ary layer. Numerical simulations for steady state conditions were conducted for free stream velocities of 10 m/s and 80 m/s. The simulation results were compared against the solutions of [3] and [15] (Figure 4 and Figure 5). The results indicated that the simulated results compares well with the analytical solution.This will be used as initial conditions from which acceleration or deceleration of the flow will be analysed.

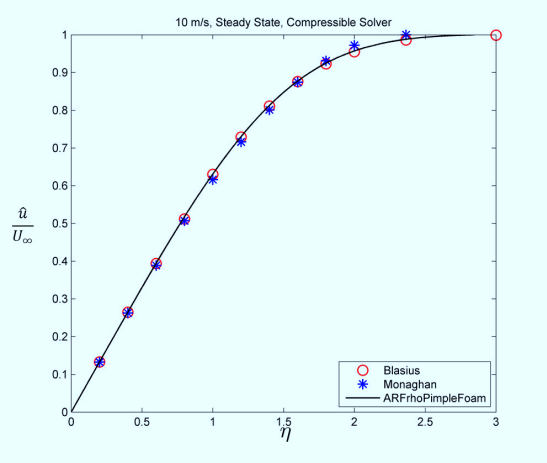

Figure 5. Steady State Solution at 10 m/s

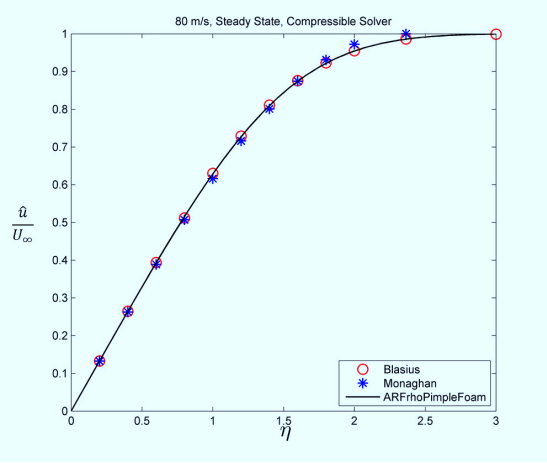

Figure 6. Steady State Solution at 10 m/s

Responses to Acceleration

Results

The accelerating flow analysis was done for the laminar flat plate. The flow was accelerated from a fully converged, steady state solution at 10 m/s to a final velocity of 80 m/s. The acceleration was from 70 g to 70000 g at increasing orders of 10. Comparisons were drawn between the non-dimensional velocity profiles at common free stream velocities for different accelerations. The results are indicated in three grouping in *Figure 18*, *Figure 19* and *Figure 20*.

Sample results that are representative of the boundary layer responses are shown for explanation purposes in *Figure 7* and *Figure 8*.

Figure 7. Sample results and observations for the lower acceleration cases

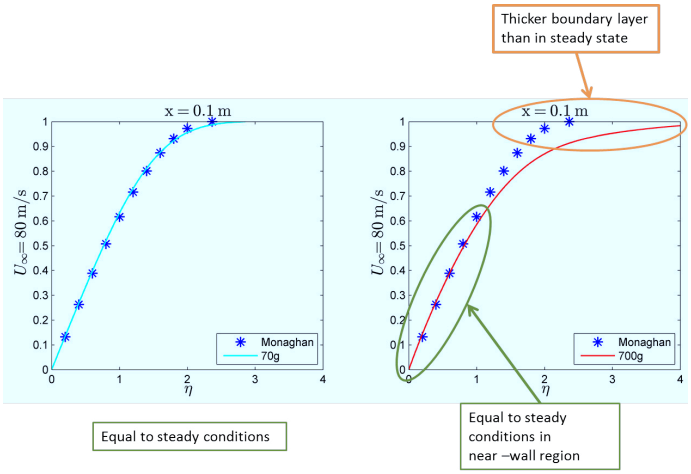

In *Figure 7* it is shown that the 70 g acceleration case remains very close to the steady state results. In the near-wall region the velocity gradient is maintained at steady state values. The boundary layer thickness is the same. In *Figure 18* it is seen that the profile deviated from the steady state conditions in the middle boundary layer region between free stream values of 17 m/s and 24 m/s, but by 38 m/s the deviations subsided and a steady profile was resumed. The diffusion term dominates the 70 g acceleration case to maintain near steady state conditions.

The 700 g acceleration case maintains the steady state profiles in the near-wall regions, but deviates as the flow approaches the free stream conditions in the far field (*Figure 7*). This leads to a thicker boundary layer than the steady state. This response is a combination of the diffusion term dominating in the near-wall region and the material derivative dominating in the far field.

The higher acceleration cases $(> \ 1000 \ g)$ is characterised by an increased velocity gradient in the near wall region resulting in a higher wall shear stress (*Figure 8*). This increase in near-wall velocity gradient is directly proportional to the acceleration - higher acceleration causes higher wall shear stresses. The boundary layer is thicker than in the steady state conditions. The flow in all regions is dominated by the momentum of the acceleration.

Figure 8. Sample results and observations for the higher acceleration cases

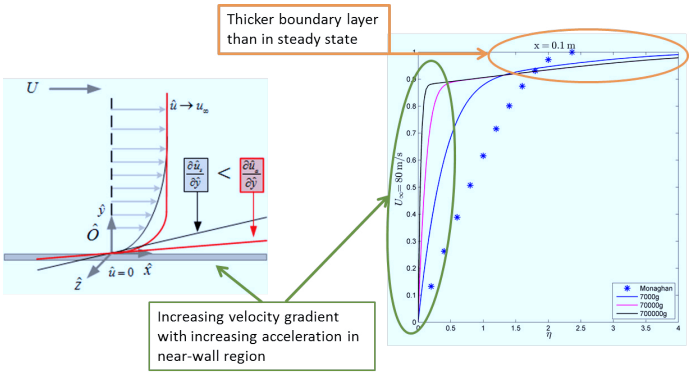

The observed behaviour is better understood in the inertial frame. In this frame the flat plate is initially in a fully developed steady state condition. The plate is moving but the far field flow is standing still. The velocity profile will have an identical shape to the velocity profile in the non-inertial frame, but the velocity at the wall will have the value of the non-inertial free stream value and the free stream in the inertial frame will be zero. As the plate accelerates the velocity at the wall will increase rapidly, and since it is not steady motion the velocity gradient near the wall will become steeper. The velocity in the free stream will however remain at zero. The thickening of the boundary layer occurs due to the momentum effects dominating the viscous effect and due to the time scale of the event being too high for the viscous effects to dominate and adjust the boundary layer flow in the changing conditions to assume the steady state profile. In the next section this mechanism will be explained mathematically.

Interpretation

The observed results can be interpreted using the boundary layer equations derived in [6]. All terms associated with rotation and translational acceleration in the y-direction is removed from the equation, resulting in the following set of boundary layer equations:

x-momentum

$$\frac{\partial \hat{\rho}\hat{u}}{\partial t} + \hat{u}\frac{\partial \hat{\rho}\hat{u}}{\partial \hat{x}} + \hat{v}\frac{\partial \hat{\rho}\hat{u}}{\partial \hat{y}} = -\frac{\partial \hat{p}}{\partial \hat{x}} + \frac{\partial}{\partial \hat{y}}\hat{\mu}\frac{\partial \hat{u}}{\partial \hat{y}} - \frac{\partial \hat{\rho} V_x}{\partial t} \qquad (8)$$

y-momentum

$$0 = -\frac{\partial \hat{p}}{\partial \hat{y}} \qquad (9)$$

The equation set above is responsible for the observed behaviour and from this a mechanism can be devised to explain the boundary layer response (*Figure 9*).

Figure 9. Boundary layer profiles for steady and accelerating conditions

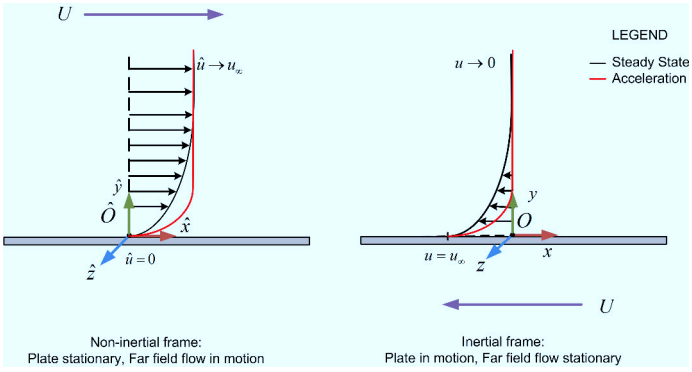

The prescribed frame velocity, here acting in the negative x-direction, acts as a source of momentum. An increase in this term on the right hand side of the momentum equation, will result in an overall increase in the material derivative on the left hand side of the equation.

$$\frac{\partial \hat{\rho}\hat{u}}{\partial t} + \hat{u}\frac{\partial \hat{\rho}\hat{u}}{\partial \hat{x}} + \hat{v}\frac{\partial \hat{\rho}\hat{u}}{\partial \hat{y}} = -\frac{\partial \hat{p}}{\partial \hat{x}} + \frac{\partial}{\partial \hat{y}}\hat{\mu}\frac{\partial \hat{u}}{\partial \hat{y}} - \frac{\partial \hat{\rho} V_x}{\partial t}$$

An increase in the material derivative results in an increase in $\hat{u}$, which in term will result in an increase in the wall velocity gradient (Figure 10) which is the observed effect in the accelerating boundary layer profile.

$$\frac{\partial \hat{\rho}\hat{u}}{\partial t} + \hat{u}\frac{\partial \hat{\rho}\hat{u}}{\partial \hat{x}} + \hat{v}\frac{\partial \hat{\rho}\hat{u}}{\partial \hat{y}} = -\frac{\partial \hat{p}}{\partial \hat{x}} + \frac{\partial}{\partial \hat{y}}\hat{\mu}\frac{\partial \hat{u}}{\partial \hat{y}} - \frac{\partial \hat{\rho} V_x}{\partial t}$$

Figure 10. Increased wall velocity gradient for accelerating conditions

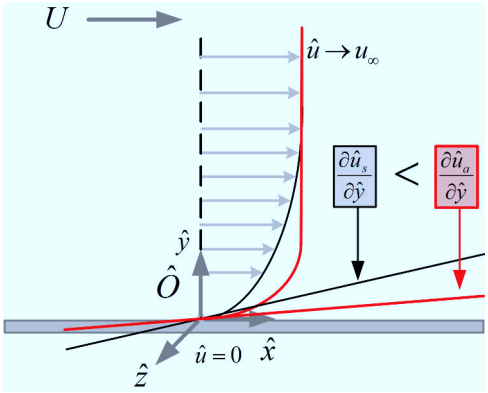

The strength of this mechanism is dependant on the magnitude of the frame acceleration. Hence, three distinct acceleration regions are identified in the translation case (*Figure 11*) as explained on the next page:

- **Region I - Viscous Dominant**. The 70 g case falls within this region. There is almost no divergence from the steady state non-dimensional result[15] which is used here for illustrative purposes. The viscous effects dominate the boundary layer flow and any disturbances in the boundary layer is neutralized by the viscous forces. This can be seen the Grouping I (Fig. 18) results at 20.5 m/s where the disturbance occurs, the upstream propagation at 24 m/s. At Grouping II (Fig. 19) 38 m/s the disturbance has been dissipated and the profile is on the steady state baseline again. In this region the rate of change in properties is small enough to allow the flow the adjust to steady state conditions. The induced momentum effects, due to acceleration, is not high enough to result in changes in the boundary layer properties.
  Acceleration Response - Type I:

Figure 11. Acceleration Response Regions by Type in Simulation Results

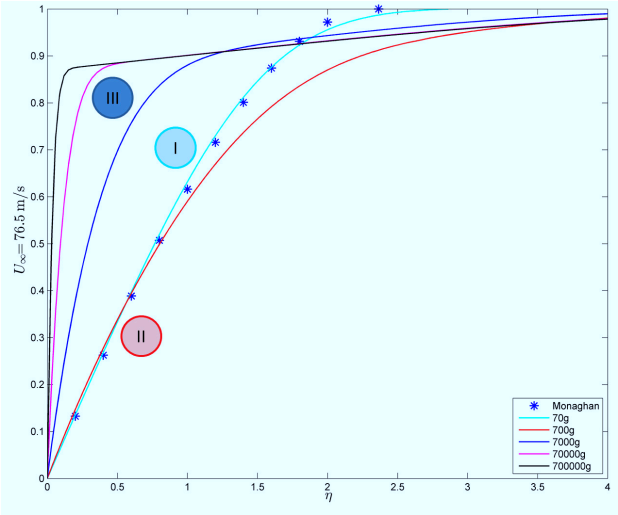

$$\frac{\partial \hat{\rho}\hat{u}}{\partial t} + \hat{u}\frac{\partial \hat{\rho}\hat{u}}{\partial \hat{x}} + \hat{v}\frac{\partial \hat{\rho}\hat{u}}{\partial \hat{y}} = -\frac{\partial \hat{p}}{\partial \hat{x}} + \frac{\partial}{\partial \hat{y}}\hat{\mu}\frac{\partial \hat{u}}{\partial \hat{y}} - \frac{\partial \hat{\rho} V_x}{\partial t}$$

- **Region II - Viscous-Momentum Interaction**. In the fluids world there is always a competition between viscous and momentum effects. The effects can't be in balance - one must dominate. In this region the viscous and momentum forces are of comparable order and causes disturbance of the boundary layer. The 700 g case falls within this region. The region (for this specific case) extends from approximately 500 g - 1100 g. It is characterized by unsteady disturbance propagation in the boundary layer.
  Acceleration Response - Type II:

$$\frac{\partial \hat{\rho}\hat{u}}{\partial t} + \hat{u}\frac{\partial \hat{\rho}\hat{u}}{\partial \hat{x}} + \hat{v}\frac{\partial \hat{\rho}\hat{u}}{\partial \hat{y}} = -\frac{\partial \hat{p}}{\partial \hat{x}} + \frac{\partial}{\partial \hat{y}}\hat{\mu}\frac{\partial \hat{u}}{\partial \hat{y}} - \frac{\partial \hat{\rho} V_x}{\partial t}$$

- **Region III - Momentum Dominant**. The three higher acceleration cases falls within this region - 7000 g, 70000 g and 700000 g. The region is characterized by a sharp increase in the near-wall velocity gradient that is directly proportional to the acceleration. The boundary layer velocity profile resembles that of a fully developed, turbulent profile with the steep gradient that becomes almost parallel with the free stream in the regions close to the boundary layer edge. An increase in boundary layer height is observed. There are definite similarities between the various profiles that can be further investigated. The general form of the profiles are comparable with similar studies in literature [1], [14].
  Acceleration Response - Type III:

$$\frac{\partial \hat{\rho}\hat{u}}{\partial t} + \hat{u}\frac{\partial \hat{\rho}\hat{u}}{\partial \hat{x}} + \hat{v}\frac{\partial \hat{\rho}\hat{u}}{\partial \hat{y}} = -\frac{\partial \hat{p}}{\partial \hat{x}} + \frac{\partial}{\partial \hat{y}}\hat{\mu}\frac{\partial \hat{u}}{\partial \hat{y}} - \frac{\partial \hat{\rho} V_x}{\partial t}$$

Responses to Deceleration

0.1 Results

The flow was decelerated from a fully converged, steady state solution at 80 m/s to a final velocity of 10 m/s. The deceleration parameter was from 70 g to 70000 g at increasing orders of 10. Comparisons were drawn between the non-dimensional velocity profiles at common free stream velocities for different decelerations. The results are shown in three grouping in *Figure 21* , *Figure 22* and *Figure 23*.

Sample results that are representative of the boundary layer responses are shown for explanation purpose in *Figure 7* and *Figure 8*.

The 70 g deceleration case remains equal to steady state conditions for the greatest part of the simulations *Figure 12* . There is a slight difference in the near-wall region, but the flow is considered to be marginally dominated by the viscosity.

Figure 12. Sample results and observations for the lower deceleration cases

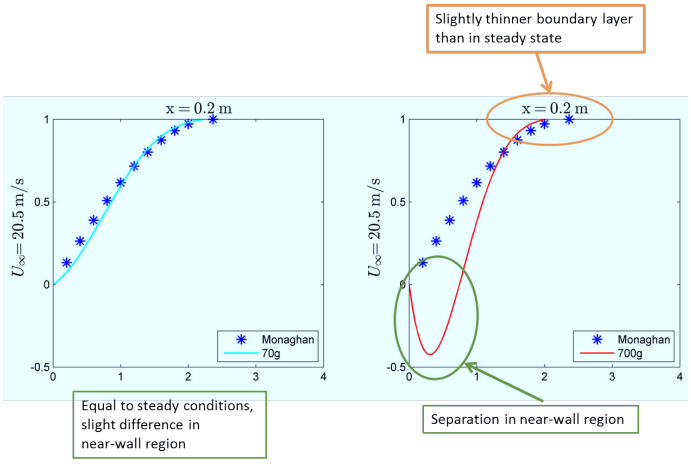

Separation is observed in the near-wall region of the 700 g case (*Figure 12*). In the far field the boundary layer is slightly thinner, but not to such a extend that the flow is fully dominated by the momentum.

In the higher deceleration cases separation is prevalent and the effect becomes increased with increasing deceleration (*Figure 13*). The boundary layer is significant thinner than the steady state as the flow is dominated by the increased momentum.

The result in this section are comparable with a study done by [1]. He obtained similar profiles by investigating the effect of inducing pressure changes in the boundary layer. In the Navier-Stokes equations, changes in acceleration will have a similar effect on the boundary layer since it is also located on the right hand side of the equation. Again the phenomenon can be best explained in the inertial frame. The plate wall has a certain velocity and the bulk flow is stationary. The velocity profile will extend

Figure 13. Sample results and observations for the higher deceleration cases

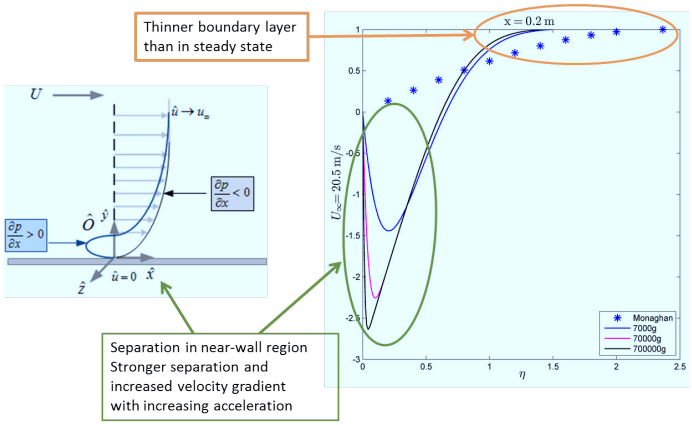

from the high velocity to zero. Now the plate is decelerated, for arguments sake let say from 80 m/s to 70 m/s. The velocity at the wall will now be 70 m/s, but due to the historic profile at 80 m/s there is a certain amount of momentum and energy in the boundary layer. This momentum and energy must go somewhere, it can not just disappear. If the acceleration is low enough the boundary layer will have time to adjust to the changing conditions and the "excess" momentum and energy will diffuse into the bulk flow. However, if the acceleration is high enough there is not time for diffusion to take place and the boundary layer has no option but to separate.

Interpretation

The observed results can be interpreted using the boundary layer equations derived in [6]. **x-momentum**

$$\frac{\partial \hat{\rho}\hat{u}}{\partial t}+\hat{u}\frac{\partial \hat{\rho}\hat{u}}{\partial \hat{x}}+\hat{v}\frac{\partial \hat{\rho}\hat{u}}{\partial \hat{y}}=-\frac{\partial \hat{p}}{\partial \hat{x}}+\frac{\partial}{\partial \hat{y}}\hat{\mu}\frac{\partial \hat{u}}{\partial \hat{y}}-\frac{\partial \hat{\rho}V_x}{\partial t} \tag{10}$$

y-momentum

$$0=-\frac{\partial \hat{p}}{\partial \hat{y}} \tag{11}$$

In this case however, the acceleration terms on the right hand side of the equation becomes a sink which causes the separation of the flow (*Equation 14*).

The deceleration of the relative frame causes a momentum sink on the right hand side of the momentum equation. This leads to a decrease on the left hand side in the material derivative.

$$\frac{\partial \hat{\rho}\hat{u}}{\partial t}+\hat{u}\frac{\partial \hat{\rho}\hat{u}}{\partial \hat{x}}+\hat{v}\frac{\partial \hat{\rho}\hat{u}}{\partial \hat{y}}=-\frac{\partial \hat{p}}{\partial \hat{x}}+\frac{\partial}{\partial \hat{y}}\hat{\mu}\frac{\partial \hat{u}}{\partial \hat{y}}-\frac{\partial \hat{\rho}V_x}{\partial t}$$

The decrease of the material derivative lead to a decrease in $\hat{u}$, which in turn causes a decrease in the velocity gradient at the wall.

Figure 14. Boundary layer profiles for steady and deceleration conditions

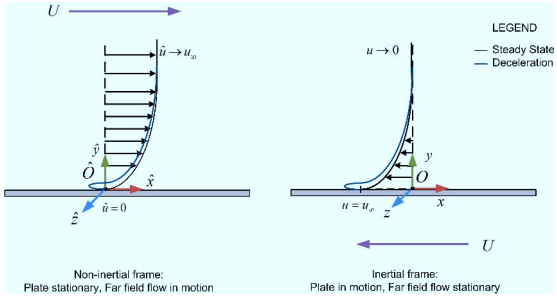

$$\frac{\partial \hat{\rho}\hat{u}}{\partial t}+\hat{u}\frac{\partial \hat{\rho}\hat{u}}{\partial \hat{x}}+\hat{v}\frac{\partial \hat{\rho}\hat{u}}{\partial \hat{y}}=-\frac{\partial \hat{p}}{\partial \hat{x}}+\frac{\partial}{\partial \hat{y}}\hat{\mu}\frac{\partial \hat{u}}{\partial \hat{y}}-\frac{\partial \hat{\rho}V_x}{\partial t}$$

A decrease in the near-wall velocity gradient causes and increase in the pressure gradient, since the terms have opposite signs. The pressure gradient increases to such an extent that an adverse pressure gradient forms and the flow separates.

$$\frac{\partial \hat{\rho}\hat{u}}{\partial t}+\hat{u}\frac{\partial \hat{\rho}\hat{u}}{\partial \hat{x}}+\hat{v}\frac{\partial \hat{\rho}\hat{u}}{\partial \hat{y}}=-\frac{\partial \hat{p}}{\partial \hat{x}}+\frac{\partial}{\partial \hat{y}}\hat{\mu}\frac{\partial \hat{u}}{\partial \hat{y}}-\frac{\partial \hat{\rho}V_x}{\partial t}$$

Figure 15. Adverse pressure gradient for decelerating conditions

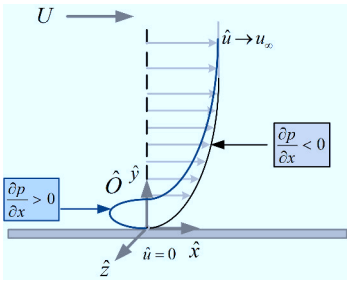

The same three distinct regions that were identified in the accelerating case, presented itself here *Figure 16*:

- **Region I - Viscous Dominant**. The 70 g case falls within this region. In comparison with the steady state non-dimensional result, there is no observed difference in the profile. The time scale at which the event occurs is low enough to allow time for the viscous forces in the boundary layer to adjust to the changes and keep the steady state profile.
  Deceleration Reaction - Type I:

$$\frac{\partial \hat{\rho}\hat{u}}{\partial t}+\hat{u}\frac{\partial \hat{\rho}\hat{u}}{\partial \hat{x}}+\hat{v}\frac{\partial \hat{\rho}\hat{u}}{\partial \hat{y}}=-\frac{\partial \hat{p}}{\partial \hat{x}}+\frac{\partial}{\partial \hat{y}}\hat{\mu}\frac{\partial \hat{u}}{\partial \hat{y}}-\frac{\partial \hat{\rho}V_x}{\partial t}$$

- **Region II - Viscous-Momentum Interaction**. The 700 g deceleration case falls within this region. The region is characterized by disturbances in the boundary layer due to the interaction between the viscous and momentum effects. Separation of the boundary layer occurs almost immediately and are directly proportional to the acceleration. In the near-wall regions the momentum effects dominates, while the close to the boundary layer edge, the viscous effects dominate. In the upper regions of the boundary layer the profile conforms to the steady state result.
  Deceleration Response - Type II:

$$\frac{\partial \hat{\rho}\hat{u}}{\partial t} + \hat{u}\frac{\partial \hat{\rho}\hat{u}}{\partial \hat{x}} + \hat{v}\frac{\partial \hat{\rho}\hat{u}}{\partial \hat{y}} = -\frac{\partial \hat{p}}{\partial \hat{x}} + \frac{\partial}{\partial \hat{y}}\hat{\mu}\frac{\partial \hat{u}}{\partial \hat{y}} - \frac{\partial \hat{\rho} V_x}{\partial t}$$

- **Region III - Momentum Dominant**. The three higher acceleration cases falls within this region. The momentum effects due to acceleration dominates here. Separation occurs very early and the boundary layer remains separated thought out the plate. The velocity gradient close to the wall is very steep and directly proportional to the acceleration. The boundary layer height is decreased with almost the same distance for all the cases in this region. Similarity, that will depend on the time scales involved, is present in the region.
  Deceleration Response - Type III:

$$\frac{\partial \hat{\rho}\hat{u}}{\partial t} + \hat{u}\frac{\partial \hat{\rho}\hat{u}}{\partial \hat{x}} + \hat{v}\frac{\partial \hat{\rho}\hat{u}}{\partial \hat{y}} = -\frac{\partial \hat{p}}{\partial \hat{x}} + \frac{\partial}{\partial \hat{y}}\hat{\mu}\frac{\partial \hat{u}}{\partial \hat{y}} - \frac{\partial \hat{\rho} V_x}{\partial t}$$

Figure 16. Acceleration Response Regions by Type in Simulation Results

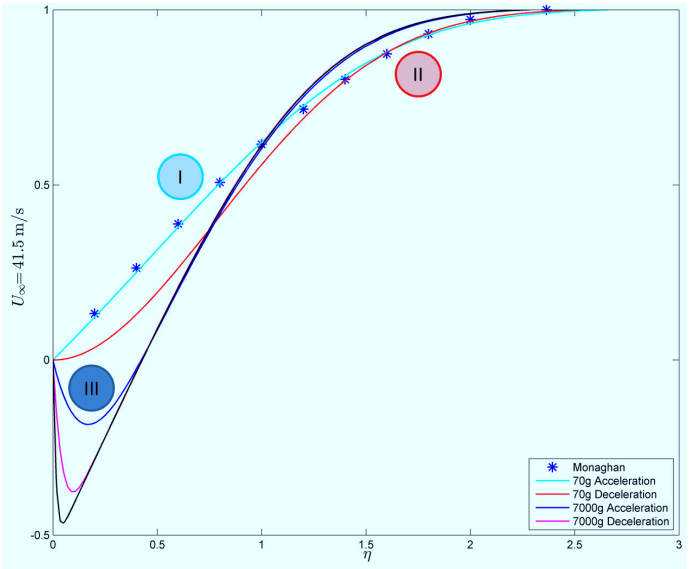

CONCLUSION

The aim of this work was to characterize the response of the laminar boundary layer to arbitrary translations. Three types of responses have been identified:

- Response Type I, which is viscous dominant. The time scale at which the event occurs is low enough to allow time for the viscous forces in the boundary layer to adjust to the changes and keep the steady state profile.
- Response Type II, which is certain regions in the boundary layer are dominated by viscosity and other regions by momentum. In acceleration the viscosity dominates in the near-wall region and momentum in the far field regions. In deceleration momentum dominates in the near-wall region and viscosity in the far field.
- Response Type III, which is dominated by momentum. The time scale at which the event occurs is too high for viscous forces in the boundary layer to adjust to the changes and keep the steady state profile. In acceleration the near-wall velocity profile increases with increasing acceleration. In deceleration separation occurs at a result of momentum changes in the flow.

In conclusion Figure 16 is presented to depict the variability in the boundary layer profiles for different initial and acceleration conditions. The flow history has an influence on the boundary layer behaviour and must be considered in aerodynamic studies.

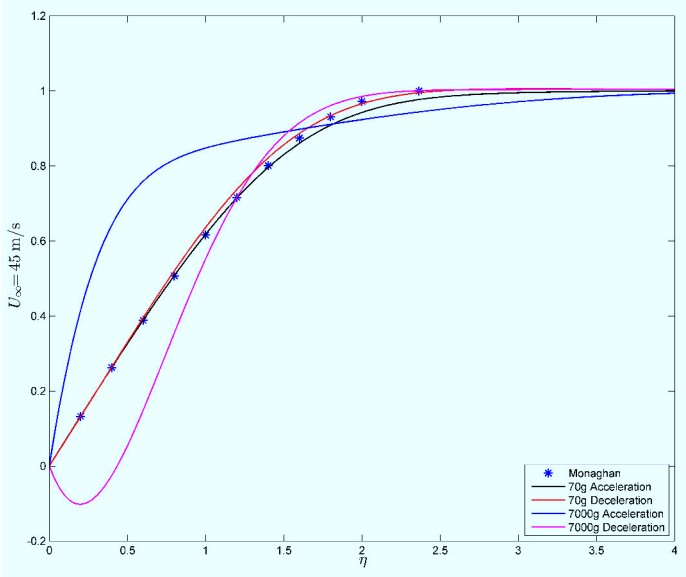

Figure 17. Variability in boundary layer profiles for different starting and acceleration conditions

REFERENCES

[1] L. Back, Accelerating and cooling effects in laminar boundary layers - subsonic, transonic and supersonic speeds. *AIAA Journal*, 8(4):974802, 1970.

[2] G.K.Batchelor, An Introduction to Fluid Mechanics. *Cambridge University Press*, Cambridge, UK, 1967.

[3] H. Blasius, Grenzschichten in flssigkeiten mit kleiner reibung. *Z. Angew. Math. Phys.*, 56:137, 1908.

[4] V. Bogdanova, Universal equations of the laminar boundary layer on a rotating blade. *Fluid Dynamics*, 6(2):251259, 1971.

[5] M.L.. Combrinck, L.N. Dala, and I.I. Lipatov, Eulerian derivation of non-inertial navier-stokes equations for compressible flow in constant, pure rotation. *Conference Paper, HEFAT*, 2015.

[6] M.L.. Combrinck, Arbitrary accelerating flow - response of the boundary layer. *PhD Thesis, University of Pretoria*, unpublished.

[7] C. Crowe, D. Elger, and J. Roberson, Engineering Fluid Mechanics. *Wiley and Sons*, 7th edition, 2001.

[8] H. Dwyer, Calculation of unsteady and three dimensional boundary layer flows. *AIAA Journal*, 11(6):773774, 1973.

[9] J. Ferziger and M. Peric, Computational Methods for Fluid Dynamics. Springer, 3rd edition, 2001.

[10] D.T.Greenwood, Principles of Dynamics. *Prentice-Hall*, Second Edition, 1988.

[11] GNU. Offcial website. GNU General Public License, urlhttp://www.gnu.org/licenses/gpl-3.0.en.html, 2016.

[12] A. Kageyama and M. Hyodo, Eulerian derivation of the coriolis force. Geochemistry, Geophysics and Geosystems, 7(2):15, 2006.

[13] A. Mager, Laminar Boundary Layer Problems Associated with Flow Through Turbomachines. *PhD thesis, California Institute of Technology*, California, 1953.

[14] A. Mager, Three-dimensional laminar boundary layer with small cross flow. *Journal of the Aeronautical Sciences*, 21(12):1, 1954.

[15] R. Monaghan, An approximate solution of the compressible, laminar boundary layer on a flat plate. *Her Majestys Stationary Office*, London, 1953.

[16] OpenFOAM. Offcial website. OpenFOAM, urlhttp://www.openfoam.com/, 2016.

[17] R. Sontagg and C. Borgnakke, An Introduction to Computational Fluid MechanicsIntroduction to Engineering Thermodynamics. *Wiley and Sons Inc*, 1st edition, 2001.

[18] H. Versteeg andW. Malalasekera, An Introduction to Computational Fluid Mechanics. *Longman Scietific and Technical*, 1st edition, 1995.

[19] F. White, Viscous Fluid Flow. *McGraw-Hill*, 3rd edition,2006.

Appendix A: Acceleration and Deceleration Figures

Figure 18. Non-Dimensional Velocity Profiles: Translating Flat Plate - Acceleration Grouping I

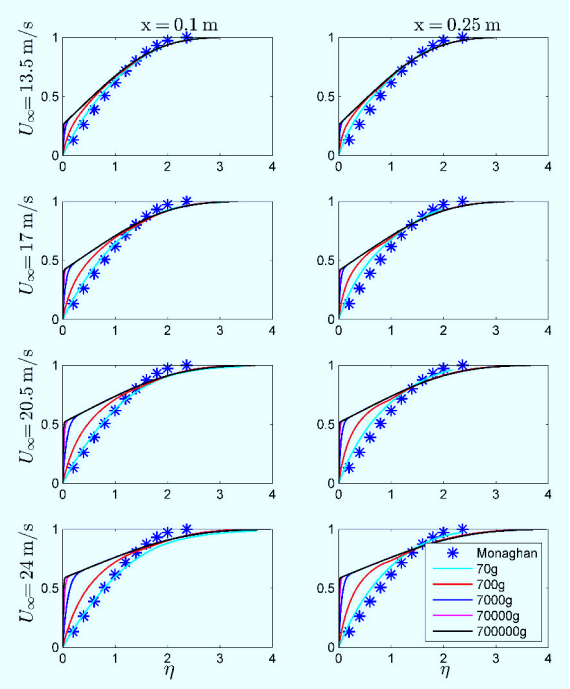

Figure 19. Non-Dimensional Velocity Profiles: Translating Flat Plate - Acceleration Grouping II

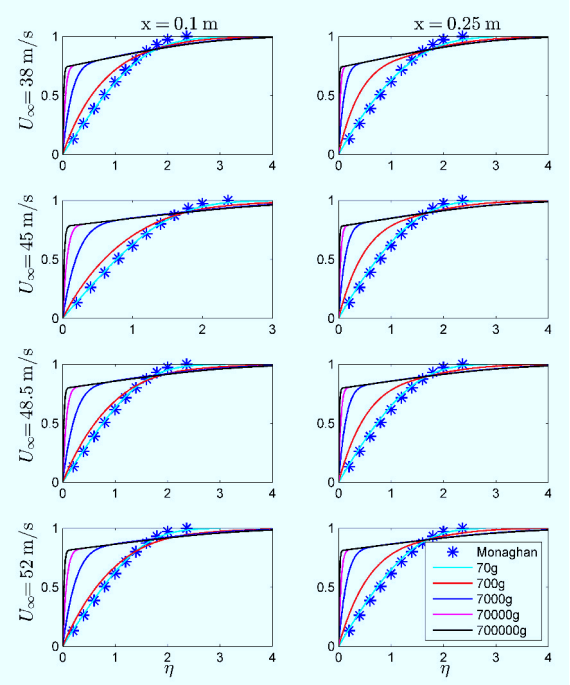

Figure 20. Non-Dimensional Velocity Profiles: Translating Flat Plate - Acceleration Grouping III

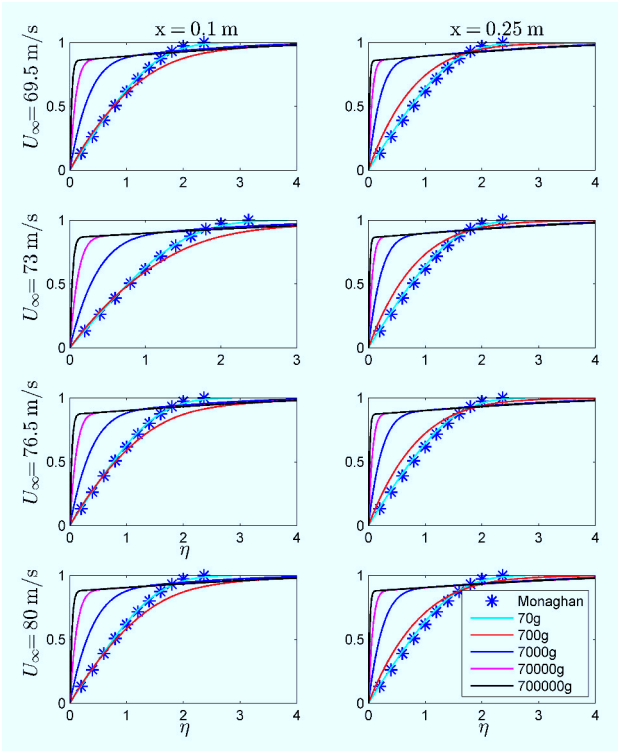

Figure 21. Non-Dimensional Velocity Profiles: Translating Flat Plate - Deceleration Grouping I

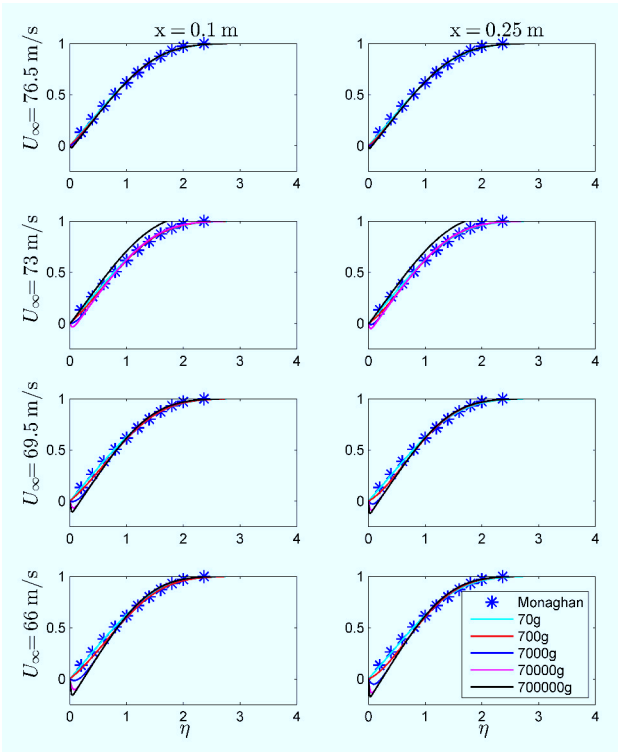

Figure 22. Non-Dimensional Velocity Profiles: Translating Flat Plate - Deceleration Grouping II

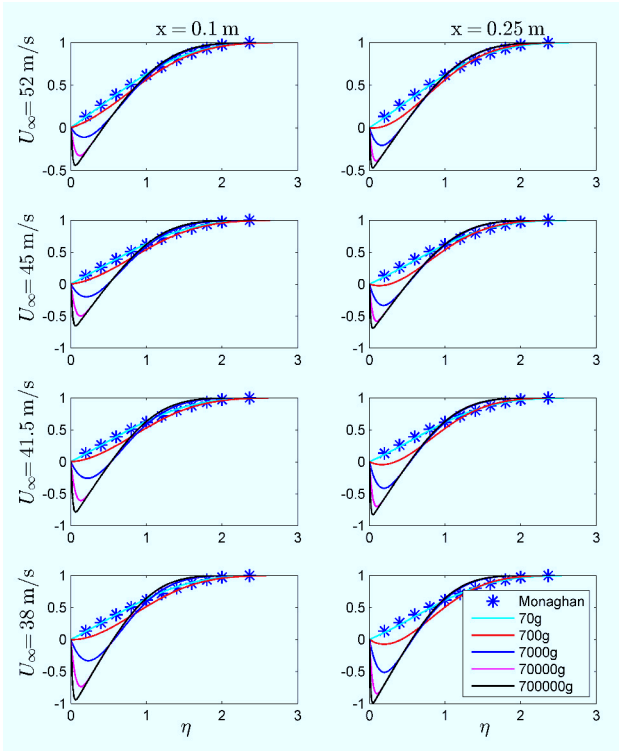

Figure 23. Non-Dimensional Velocity Profiles: Translating Flat Plate - Deceleration Grouping III